

3D Numerical Investigation of Surface Wettability Effects on Runback Water Flow Evolution on the Aero-engine Rotating Spinners

ZHU Yuanxun¹, MA Kuiyuan^{1*}, LIN Guiping^{1,2*}, JIN Haichuan², BU Xueqin²

1. Hangzhou International Innovation Institute, Beihang University, Hangzhou 311115, P. R. China;

2. School of Aeronautic Science and Engineering, Beihang University, Beijing 100191, P. R. China

(Received 15 January 2025; revised 20 May 2025; accepted 10 June 2025)

Abstract: The icing of aero-engine inlet components during flight can affect engine operational safety. Conventional hot-air anti-icing systems require a large amount of bleed air, which compromises engine performance. Consequently, low-energy anti/de-icing methods based on superhydrophobic surfaces have attracted widespread attention. Previous studies have demonstrated that for stationary components, superhydrophobic surfaces can significantly reduce anti-icing energy consumption by altering the flow behavior of runback water. However, for rotating inlet components of aero-engines, the effectiveness of superhydrophobic surfaces and the influence of surface wettability on the evolution of runback water flow remain unclear due to the effects of centrifugal and Coriolis forces. This study establishes a 3D liquid water flow simulation model using the volume of fluid (VOF) method to investigate the effects of rotational speed, airflow velocity, and surface wettability on the runback water flow behavior over the rotating spinner under dynamic rotation conditions. The results show that the rotational effects and surface wettability mutually reinforce one another. Specifically, increasing the rotational speed and contact angle can both enhance the flow velocity of liquid water and accelerate the breakup and rupture of liquid film, leading to the formation of rivulets, droplets, and subsequent detachment from the surface. A theoretical model based on force balance is proposed to describe the evolution of runback water flow, and the analysis reveals that as the rotational speed and contact angle increase, the water film is more likely to break up to form rivulets and beads, and the critical radius for droplet detachment from the surface decreases, making it easier removal from the surface.

Key words: anti-icing; runback water flow characteristics; volume of fluid (VOF) method; surface wettability; rotating surface

CLC number: V211

Document code: A

Article ID: 1005-1120(2025)05-0679-14

0 Introduction

When an aircraft flies through clouds containing supercooled water droplets, icing occurs on aero-engine inlet components, leading to flow passage blockage, thrust reduction, and adverse effects on engine efficiency. In extreme circumstances, this may cause engine surge, posing a significant threat to flight safety. Given the structural complexity of aero-engines, multiple components are susceptible to ice accretion, including inlet lips, struts, guide vanes, splitter rings, as well as rotating compo-

nents such as rotating spinners and fan blades. Among these components, the rotating spinners experience the most severe ice accretion due to their relatively high rotational speeds and large areas for supercooled droplet impingement. The ice accretion process and ice shapes on rotating spinners differ significantly from those on stationary surfaces, often forming needle-like or feather-like structures. Previous studies have demonstrated^[1] that the formation of these unique ice shapes is related to the liquid water flow evolution behavior on the surface under the

*Corresponding authors, E-mail addresses: ky.ma@buaa.edu.cn; gplin@buaa.edu.cn.

How to cite this article: ZHU Yuanxun, MA Kuiyuan, LIN Guiping, et al. 3D numerical investigation of surface wettability effects on runback water flow evolution on the aero-engine rotating spinners[J]. Transactions of Nanjing University of Aeronautics and Astronautics, 2025, 42(5): 679-692.

<http://dx.doi.org/10.16356/j.1005-1120.2025.05.010>

coupled effects of centrifugal force and aerodynamic drag^[2]. To ensure flight safety, it is necessary to conduct research on the icing of rotating surfaces^[3]. Due to the unique geometric structure of rotating spinners, researchers have proposed several new low-energy anti-icing methods for engine components, such as rotating heat pipe^[4], structural anti-icing designs^[5], and superhydrophobic surface anti-icing. The superhydrophobic anti-icing method modifies the surface to achieve superhydrophobicity utilizing its wettability to prevent icing, thereby reducing system energy consumption^[6-7]. Our previous research^[6-9] have systematically investigated low-energy anti-icing mechanisms on superhydrophobic surfaces, revealing that surface wettability alterations induce distinctive liquid water flow behaviors, spreading, and detachment on rotating surfaces. Therefore, further investigation into the fundamental physics governing runback water flow evolution on rotating spinners with different wettabilities is necessary.

Experimentally, Yuan et al.^[10] and Zhang et al.^[11] observed the characteristics of water film flow. Due to limitations in experimental setups and observation methods, many researchers have turned to simulation studies. Classical models such as the Messinger model^[12], the shallow water icing model (SWIM) proposed by Messinger^[13], the Myers model^[14], and the improved Myers model by Gori et al.^[15] have provided insights into the mechanisms of water film flow on icing surfaces from different perspectives. Zheng et al.^[16] used the volume of fluid (VOF) method to simulate 2D runback water on anti-icing surfaces. Thompson et al.^[17] used force balance (FB) analysis method to study wind-driven rivulet flow and El-Genk et al.^[18] used a finite element numerical method to improve the minimization of total energy (MTE) method.

Most studies on the effects of wettability on water film flow characteristics have been conducted on stationary surfaces rather than rotating surfaces. Yang et al.^[19] and Dong et al.^[20-21] studied the flow characteristics of water films on different surfaces. However, their study only considered static anti-icing characteristics and did not address rotating conditions.

The Coriolis and centrifugal forces also affect the water film flow with the component rotates. Jian

et al.^[22-23] introduced a water film detachment model for rotating component surfaces and studied the effects of Coriolis and centrifugal forces on the external sparse gas-liquid two-phase flow and the water film on rotating surfaces. Chen et al.^[24] modified the solution for water film velocity with centrifugal force on rotating component surfaces. Wang et al.^[25-26] modified the Messinger model to consider the effect of centrifugal force on the distribution of uncondensed water and applied it on rotating turbine blade surfaces. Hamed et al.^[27] used the Lagrangian method to solve the airflow field in compressor blade passages and solved the droplet trajectories in the flow field in a rotating cylindrical coordinate system. Wang et al.^[28] simulated the flow field around a rotor, considering the effects of Coriolis and centrifugal forces in the air phase solution process.

Understanding how surface wettability affects runback ice formation and the role of surface wettability in anti-icing and de-icing processes is the key to mastering low-energy anti-icing mechanisms. Detailed studies on droplet flow characteristics and ice accretion and anti-icing mechanisms on icing surfaces are needed, especially in real 3D rotating component environments. First, the rotational effect of rotating components in engines affects droplet impingement and water film flow characteristics, which means that it is necessary to study the effect of wettability on the flow characteristics of liquid water under centrifugal force. Second, the influence of wettability on runback water flow pattern is closely related to the anti-icing mechanism of superhydrophobic surfaces and requires further study. Due to the lack of accurate theoretical analysis of water film flow characteristics and precise measurement techniques to quantify transient water film flow behavior on rotating component surfaces, the effects of surface wettability on water film flow evolution on 3D rotating components remain unclear, leaving a research gap that needs to be addressed.

To address these issues, this study utilizes the VOF method in conjunction with a 3D rotating coordinate system to establish the runback water flow simulation model and investigate the effects of surface wettabilities on runback water flow evolution on rotating spinner surfaces. Furthermore, a theoretical analysis based on the FB is conducted to ex-

plore the coupling effects of rotational dynamics and surface wettabilities on the evolution behavior of runback water on rotating surfaces. The influence of surface wettability on the breakup of water films into rivulets and the subsequent rupture of rivulets into droplet flow, as well as the detachment of droplet flow from the surface, is thoroughly investigated.

1 Simulation Method

1.1 VOF calculation model in a rotating coordinate system

2D simulations are insufficient to capture the continuous liquid film break up in the spanwise direction. In contrast, a 3D simulation model using the VOF method^[29] can reveal the transient behavior and evolution characteristics of liquid water flow on surfaces with different wettabilities under high-speed airflow shear forces. The energy transfer is not considered in this study, and the liquid water flow characteristics under isothermal conditions are calculated.

To consider the effects of rotation, a rotating non-inertial reference frame is introduced. The reference frame takes the rotation axis of the spinner as its central axis and rotates around this axis at the same time angular velocity as the spinner. Under this transformation, the fluid velocity is expressed as

$$\mathbf{u}_m = \mathbf{u} - \mathbf{u}_r = \mathbf{u} - \boldsymbol{\omega} \times \mathbf{r} \quad (1)$$

Therefore, the governing equations for the VOF model in the rotating coordinate system are as follows

$$\frac{\partial \rho}{\partial t} + \nabla \cdot (\rho \mathbf{u}_m) = 0 \quad (2)$$

$$\frac{\partial (\rho \mathbf{u}_m)}{\partial t} + \rho (2\boldsymbol{\omega} \times \mathbf{u}_m + \boldsymbol{\omega} \times \boldsymbol{\omega} \times \mathbf{r}) + \nabla \cdot (\rho \mathbf{u}_m \mathbf{u}_m) = -\nabla p + \nabla \cdot \bar{\bar{\tau}}_m + \mathbf{F} \quad (3)$$

where ρ and \mathbf{u} are the mixture density and mixture velocity, respectively, obtained by weighted averaging based on phase volume fractions; p is the pressure, \mathbf{F} the generalized source term in the momentum equation, $\boldsymbol{\omega}$ the angular velocity, \mathbf{r} the radial vector, and $\bar{\bar{\tau}}_m$ the viscous shear stress under relative velocity. Compared with the governing equations for stationary surfaces, the rotating coordinate system uses relative velocity as the dependent variable and includes additional terms accounting for Coriolis acceleration ($2\boldsymbol{\omega} \times \mathbf{u}_m$) and centrifugal acceleration ($\boldsymbol{\omega} \times \boldsymbol{\omega} \times \mathbf{r}$).

1.2 Computational domain and boundary conditions

A rotating spinner of a certain type is selected, as shown in Fig.1. The geometric structure is a truncated front section of a spinner, modeled and simulated at a 1:2 scale compared with the actual aero-engine. The truncated base diameter is 150 mm, and the cone angle is 72° .

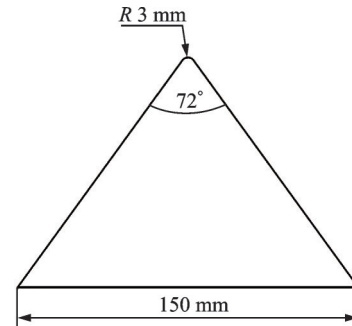


Fig.1 Model of a certain type of aero-engine rotating spinner

The commercial software Ansys Fluent is used for simulation calculations. A 3D computational domain is established, as shown in Fig.2. The surrounding flow field of the rotating spinner is mod-

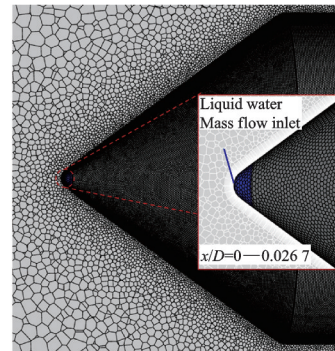
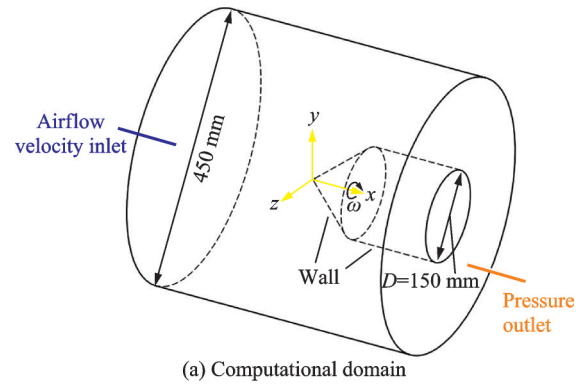


Fig.2 Schematic diagram of computational domain and boundary conditions for liquid water flow simulation on rotating surfaces

eled with a total length of 450 mm. The annular outlet has an inner diameter of 150 mm, matching the spinner base diameter, and an outer diameter of 450 mm. To optimize calculations, a 150 mm long stabilization section is added downstream of the spinner trailing edge.

For boundary conditions, the left circular end face is set as the far-field air velocity inlet, and the right annular end face is set as the pressure outlet. Liquid water is introduced through a mass flow inlet, with a rate chosen based on experimental conditions, corresponding to an equivalent liquid water content (LWC) of $(3 \pm 0.5) \text{ g/m}^3$ and yielding a water mass flow rate of 8 g/s. The inlet range is determined by FENSAP-ICE simulations of droplet collection efficiency, ensuring consistency with the impingement region. As illustrated in Fig.3, the droplet collection efficiency is the highest at the leading edge and decreases sharply to less than 0.3 at $x/D=0.0267$.

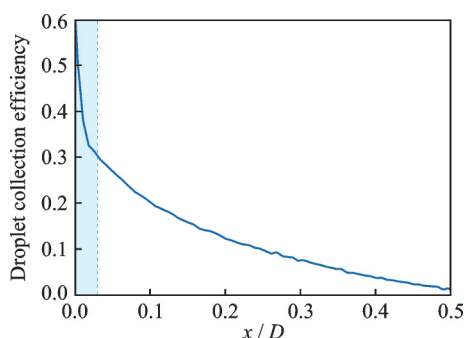


Fig.3 Change of droplet collection efficiency on rotating spinners with distance

The simulation employs the RNG $k-\varepsilon$ turbulence, with the PRESTO method used for the pressure term algorithm. The compressive schemes (a second order reconstruction scheme based on the slope limiter) is selected for interface calculations. The transient simulation is carried out over 0.4 s using a time step of 1 ms, resulting in 400 time steps.

Three grid resolutions are designed, with total cell counts of 191, 325, and 478 W. Analysis of the water film thickness (Fig.4) indicates that the 325 W grid provides an optimal balance between computational efficiency and accuracy. The refined region, which is critical for accurately resolving the water film flow behavior, has a total height of

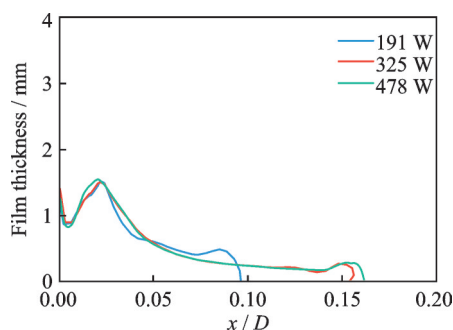


Fig.4 Grid-independent verification results

2 000 μm , and incorporates 15 layers of grid refinement near the wall.

2 Results

2.1 Verification of simulation accuracy

In order to verify the accuracy of the simulation calculations, a comparison is conducted with experimental results. As shown in Fig.5, for the 10° surface, the water film spreads uniformly and covers nearly the entire surface of the rotating spinners. In the case of the 70° surface, the rivulets can be observed, and the break location is largely consistent.

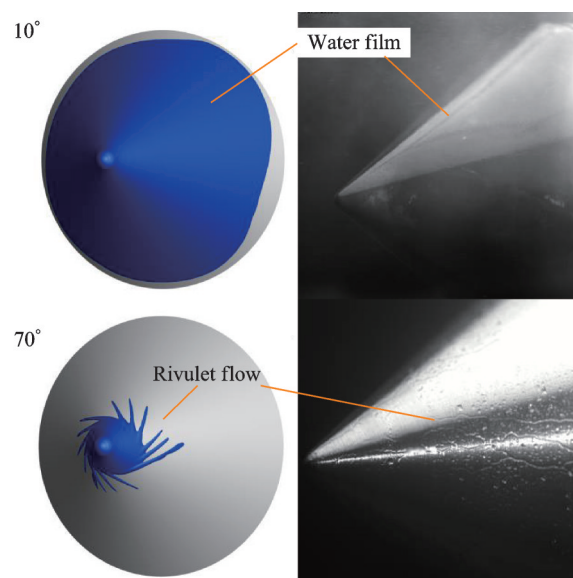


Fig.5 Comparison between simulation and experiment of surface water film flow patterns at contact angles of 10° and 70° ($U_\infty=20 \text{ m/s}$, $n=1\,000 \text{ r/min}$)

2.2 Effects of wettability on liquid water flow pattern on rotating surfaces

Figs.6—9 show the liquid water flow patterns on surfaces with different wettabilities (contact an-

gles) under a wind speed of 20 m/s and a rotational speed of 1 000 r/min. The flow pattern reaches a steady state within 0.3 s, so six time points are selected for each surface to display the flow pattern. The simulation model captures the circumferential flow spreading and rivulet formation on the rotating surface due to the rotational effect, as well as the influence of surface wettability on the flow pattern. As shown in Fig.6, on a superhydrophilic surface with a contact angle of 10° , the liquid water forms a relatively continuous film over time without rupturing into rivulets, and it almost covers the entire spinner

by $t = 0.3$ s.

As shown in Fig.7, on a surface with a contact angle of 70° , the liquid water shows obvious rivulets or liquid fingers^[30-31] at $t = 0.1$ s, where the liquid film ruptures at the thinner middle section of the spinner, forming rivulets deflected opposite to the rotation direction. Additionally at $t = 0.15$ s, drop-let flows formed by rivulet rupture can be observed. The rivulet channels on the surface remain relatively stable over time without significant changes. In the middle and rear sections of the spinner (dimensionless axial position $x/D=0.263-0.688$), the sur-

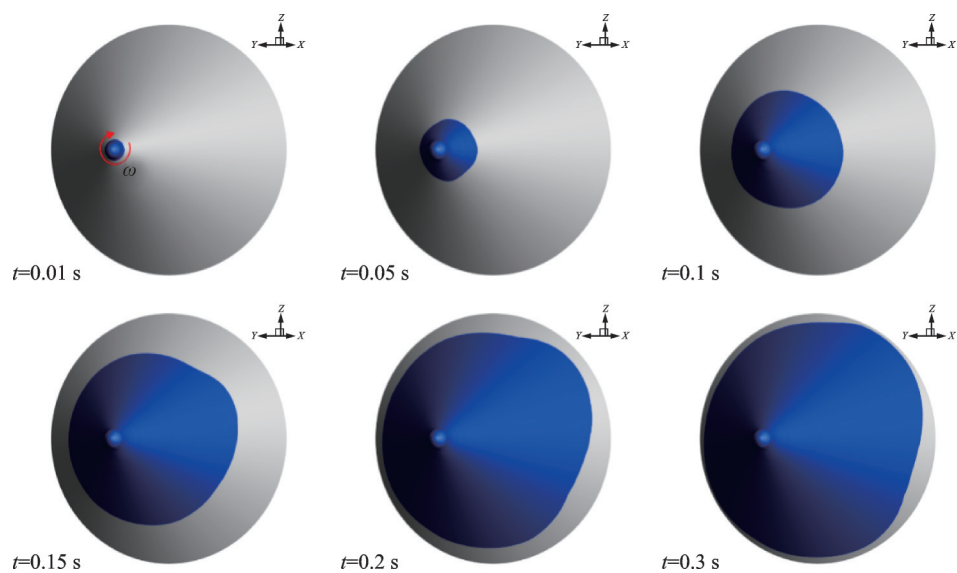


Fig.6 Liquid water flow evolution on a rotating surface with a contact angle of 10° at different moments when the incoming wind speed is 20 m/s and the rotation speed is 1 000 r/min (clockwise rotation)

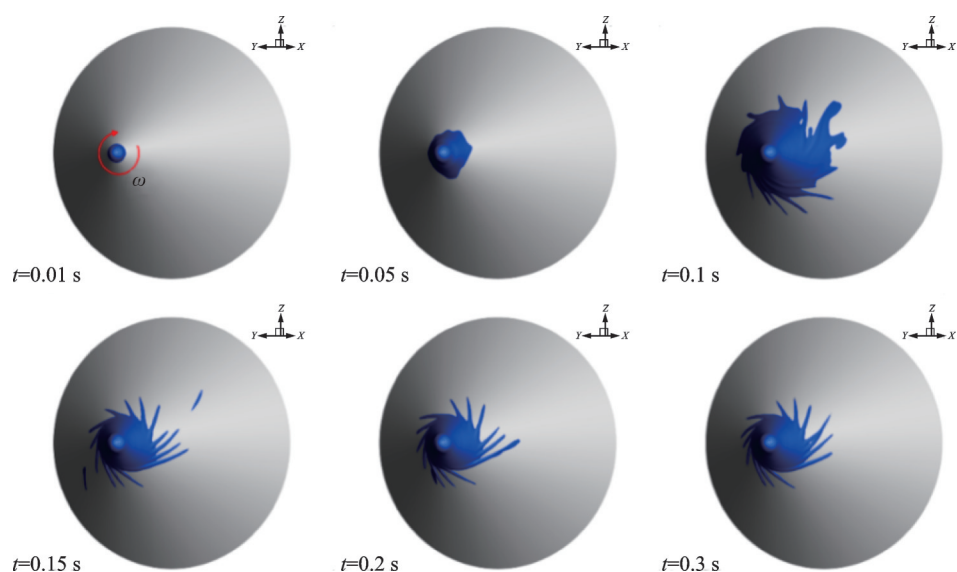


Fig.7 Liquid water flow evolution on a rotating surface with a contact angle of 70° at different moments when the incoming wind speed is 20 m/s and the rotation speed is 1 000 r/min (clockwise rotation)

face is not covered by the liquid film. This phenomenon differs slightly from experimental observations, mainly because the entire spinner surface is within the impingement zone in experiments, so some liquid water directly impinging on the surface can be observed in the middle and rear sections.

As shown in Fig.8, on a surface with a contact angle of 90° , the liquid film also forms deflected rivulets, and the frequency of droplet flows formed by rivulet rupture increases. This indicates that as the

contact angle increases, the liquid water on the rotating spinner surface is more likely to transition from a continuous film to rivulets and droplet flows, consistent with observations on stationary surfaces. As shown in Fig.9, on a superhydrophobic surface with a contact angle of 150° , the liquid water coverage area is significantly smaller than those on other surfaces (dimensionless axial position $x/D=0-0.1$), and the formation of rivulets is suppressed, with no obvious rivulets observed in the simulation.

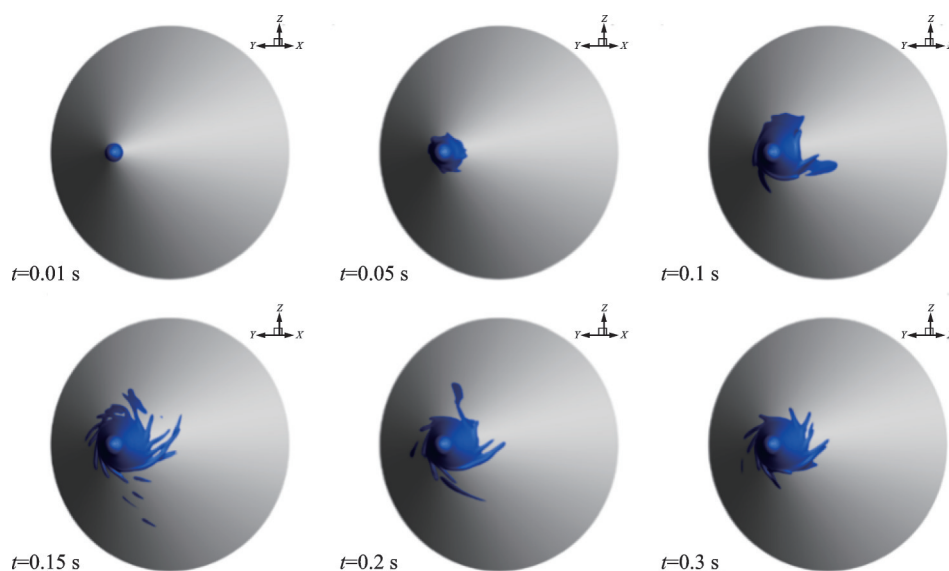


Fig.8 Liquid water flow evolution on a rotating surface with a contact angle of 90° at different moments when the incoming wind speed is 20 m/s and the rotation speed is 1 000 r/min (clockwise rotation)

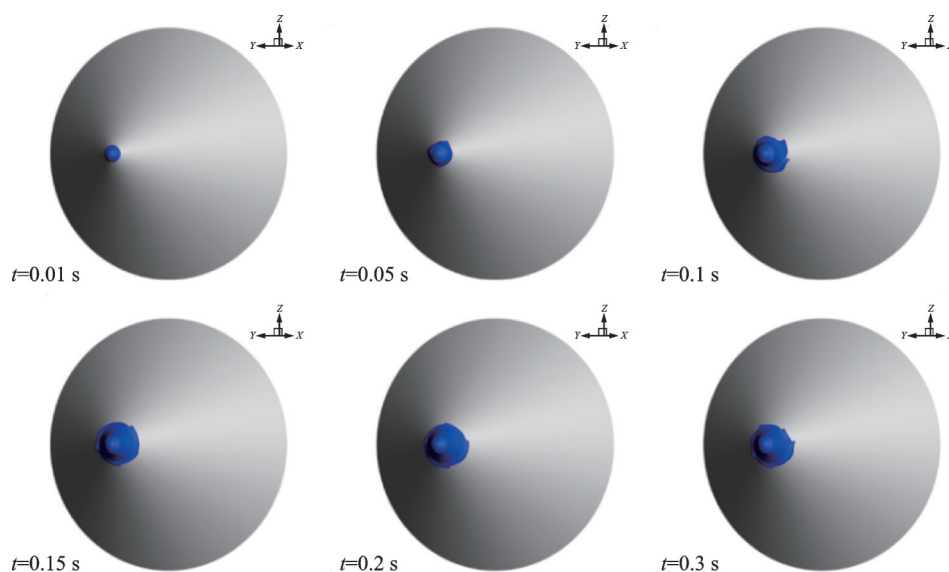


Fig.9 Liquid water flow evolution on a rotating surface with a contact angle of 150° at different moments when the incoming wind speed is 20 m/s and the rotation speed is 1 000 r/min (clockwise rotation)

The farthest coverage positions of liquid water on the four surfaces are extracted, and the quantitative data are shown in Fig.10. As the contact angle increases, the coverage position and area of liquid water decrease, and the liquid water detaches from the surface earlier. From an anti-icing perspective, a larger contact angle means that the surface area requiring protection on the rotating spinner is smaller, reducing the heat and bleed air required for anti-icing.

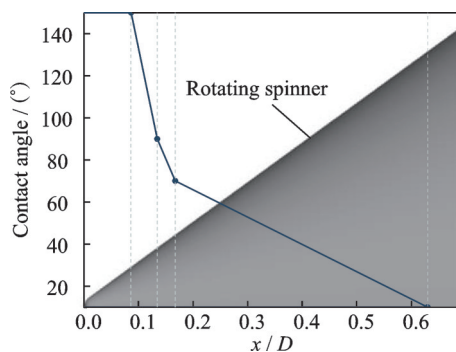


Fig.10 Relationship between the farthest dimensionless axial position (x/D) of liquid water coverage and contact angle

Extracting the water film thickness distribution on surfaces with different contact angles, as shown in Fig.11, reveals that the film thickness remains below 2 mm. During the runback process, the water film thickness gradually decreases along the flow direction. On the superhydrophilic surface with a 10° contact angle, the film thickness continuously decreases, maintaining a uniform thickness of approximately $500\ \mu\text{m}$, whereas on surfaces with contact angles of 70° , 90° , and 150° , water film breakup and rupture occur, leading to an increase in thick-

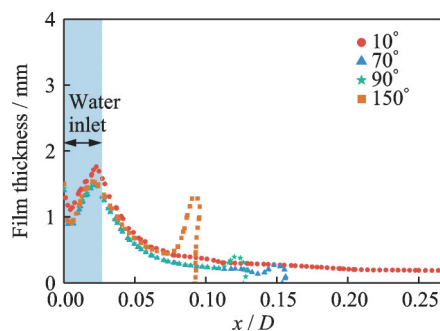


Fig.11 Water film thickness distribution along the axial direction on surfaces with different contact angles

ness near the advancing contact line and the formation of bulges. Moreover, the height of bulges increases with the contact angle. This phenomenon will be discussed further in the theoretical analysis in Section 2.4.

2.3 Effects of rotational speed and wind speed on liquid water flow

Fig.12 shows the liquid water flow patterns on a rotating spinner with a contact angle of 70° under different rotational speeds at a wind speed of 50 m/s.

As shown in Fig.12(a), at a rotational speed of 1 000 r/min, the liquid film spreads on the surface under relatively high wind speed, forming rivulets during the runback flow process. The deflection angle of the rivulets is smaller compared with low wind speed conditions, mainly because the rivulet deflection angle is related to the ratio of rotational linear velocity to incoming flow velocity. When the rotational speed increases, as shown in Figs.12(b) and (c), no rivulets are observed on the spinner surface, and the liquid film coverage area is closer to the leading-edge stagnation point. This is because a higher rotational speed results in a greater centrifugal force on the liquid water, causing it to detach from the surface near the leading edge without forming rivulets. On rotating surfaces, when the wind speed and rotational speed are low, the linear velocity generated by rotation promotes rivulet formation. However, when the rotational speed further increases, the centrifugal force on the liquid film can cause it to detach from the surface, suppressing rivulet formation and favoring anti-icing under consistent conditions.

Fig.13 shows the liquid water flow pattern on a rotating superhydrophobic spinner with a contact angle of 150° under different incoming flow velocities at a rotational speed of 4 000 r/min. As shown in Fig.13(a), under low wind speed conditions, the effect of rotational linear velocity on flow pattern is significant, with obvious rivulets and large deflection angles. As the incoming flow velocity increases, the effect of rotational speed on the relative velocity of liquid water decreases, and the aerodynamic drag directly caused by the incoming flow domi-

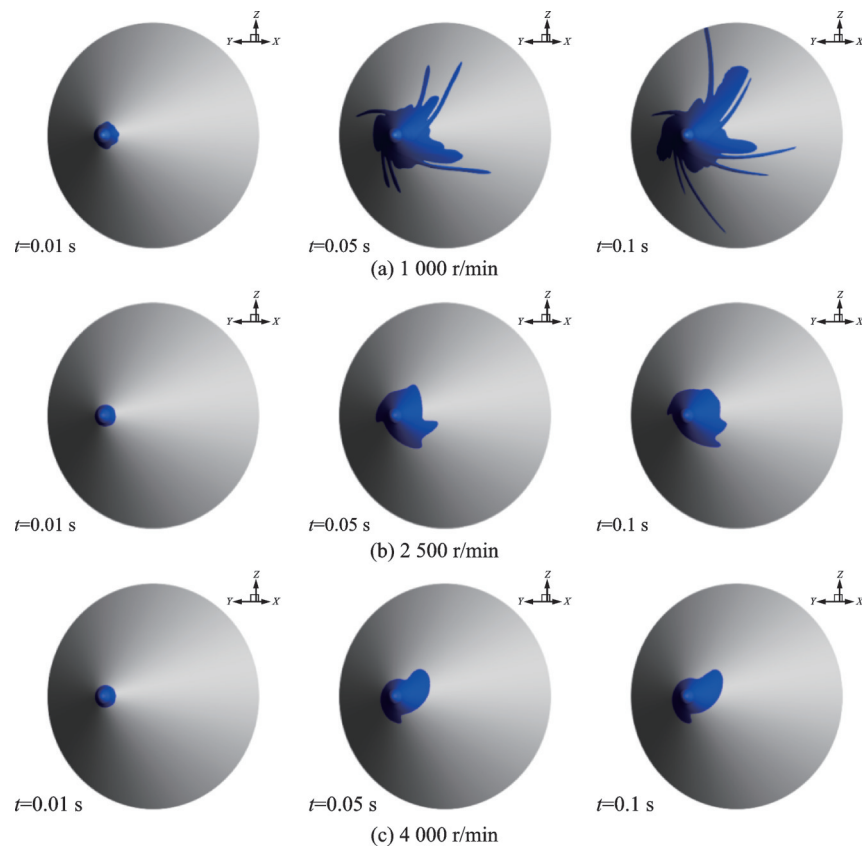


Fig.12 Comparison of liquid water flow evolution on a rotating spinner with a contact angle of 70° under different rotational speeds at a wind speed of 50 m/s

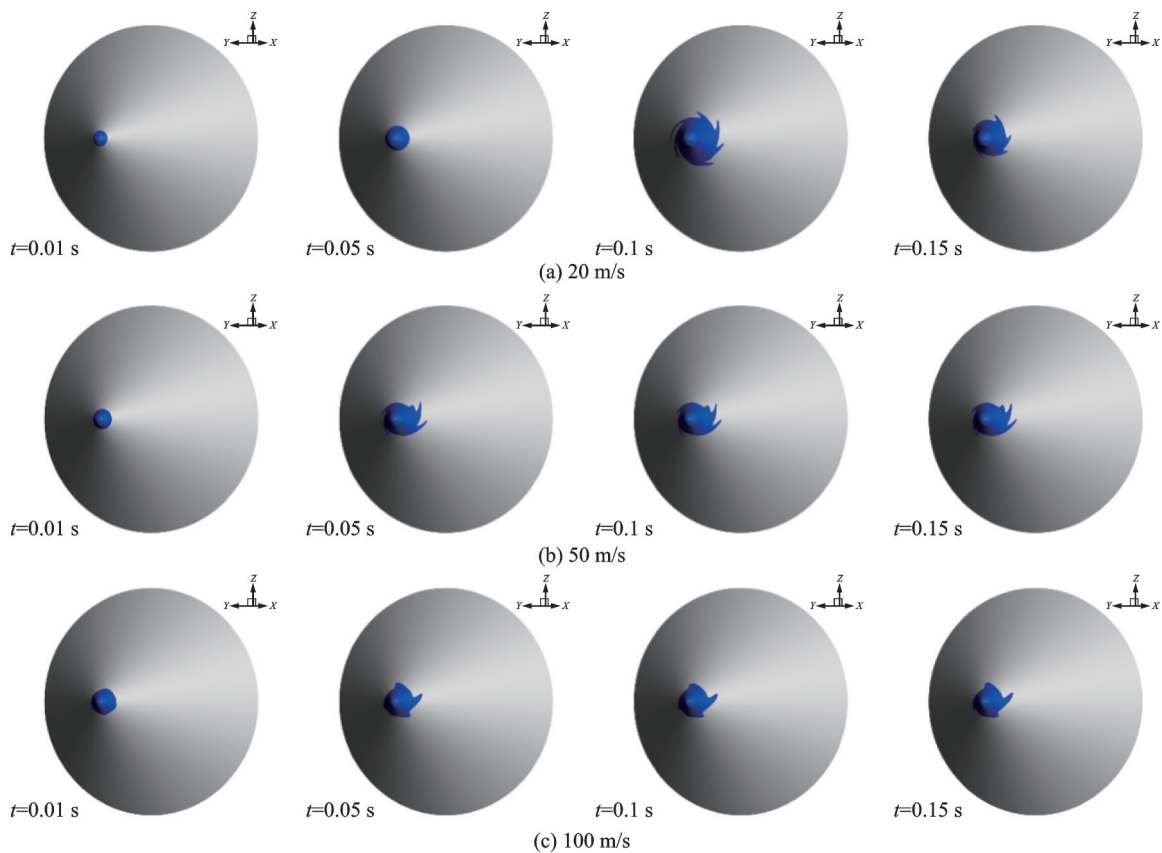


Fig.13 Comparison of liquid water flow evolution on a rotating superhydrophobic surface with a contact angle of 150° under different wind speeds at a rotational speed of $4\,000 \text{ r/min}$

rates. Therefore, the number of rivulets decreases with increasing wind speed, and the deflection angle decreases. Even under high wind speed and high rotational speed conditions, the liquid water coverage area on the superhydrophobic surface is relatively small, indicating that surface tension and wettability have a significant impact on liquid water flow pattern.

2.4 Theoretical model analysis of water film/rivulet flow based on FB method

To further analyze the effect of surface wetta-

bility on water film/rivulet flow on rotating surfaces, a theoretical model based on FB analysis is developed. Due to the rotational effect, the presence of centrifugal force changes the force balance on the water film, leading to different flow evolution behaviors. The physical model is selected as shown in Fig.14. Since the relative velocity between the water film and the spinner surface is small, the Coriolis force is neglected. The angle between the rotation axis and the wall is α . The FB for rivulet flow in the direction parallel to the wall and incoming flow is

$$F_{D,x} + F_{o,x} = F_{\sigma,x} \quad (4)$$

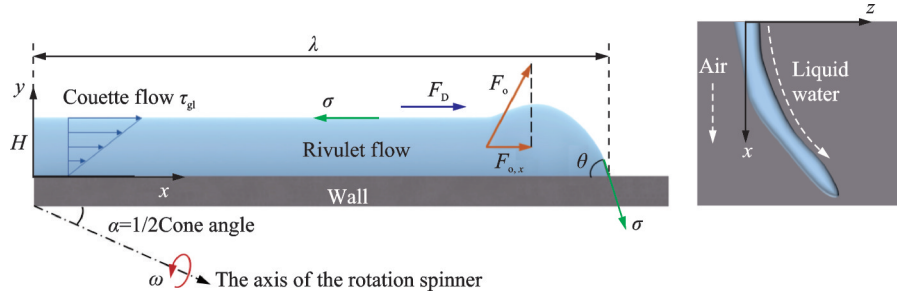


Fig.14 Physical model and force analysis of water film/rivulet flow on rotating surfaces

The component of centrifugal force per unit width along the surface and parallel to the incoming flow direction $F_{o,x}$ is

$$F_{o,x} = \rho_l \lambda H \omega^2 r_o \sin \alpha \cos \left(\arctan \frac{\omega r_o}{U_\infty} \right) \quad (5)$$

where λ is the characteristic length for unbalanced aerodynamic shear force, approximately taken as $\lambda = 168H^{[32]}$; and r_o is the centrifugal radius, which increases as the water film flows runback on the rotating spinner. The aerodynamic resistance (shear force) is the driving force when considering the flow of the water film/stream. Simplifying the net surface tension and the aerodynamic resistance to a 2D problem, we have

$$F_D = \frac{1}{2} \rho_g U_\infty^2 C_D \Delta h \quad (6)$$

$$F_{\sigma,x} = \sigma(1 - \cos \theta) \quad (7)$$

where ρ_g is the density of the gas; C_D is the aerodynamic drag coefficient; σ the height of the head bulge; and Δh the surface tension coefficient. From the FB, we have

$$\rho_l \omega^2 r_o 168 H^2 \sin \alpha \cos \left(\arctan \frac{\omega r_o}{U_\infty} \right) + C_D \frac{1}{2} \rho_g U_\infty^2 \Delta h = \sigma(1 - \cos \theta) \quad (8)$$

where ρ_l is the density of the liquid.

Substituting the operating conditions (wind speed $U_\infty = 20$ m/s, $\alpha = 36^\circ$, the drag coefficient $C_D = 0.6^{[33]}$) and relevant constants, the equation becomes

$$147 \Delta h + 98748 \omega^2 r_o H^2 = 0.0728(1 - \cos \theta) \quad (9)$$

Fig.15 shows the relationship between the critical water film thickness and bulge height for rivulet flow under different rotational speeds and contact angles at a centrifugal radius of 0.02 m. The physical meaning of the curves is the critical state for the transition of water film/rivulet flow from stagnation to flow. When the rivulet flow thickness and bulge height exceed the critical value, the water film/rivulet flow will move. At the same time, the increase in thickness causes the water film to contract in the spanwise direction, leading to spanwise rupture and rivulet formation. As the rotational speed increases, the curve contracts toward the lower-left corner, and the critical thickness and bulge height decrease. This means that the liquid film is more prone to flow and form the rivulet flow under the additional aerodynamic shear force and centrifugal force caused by rotation. On stationary spinner surfaces, the liq-

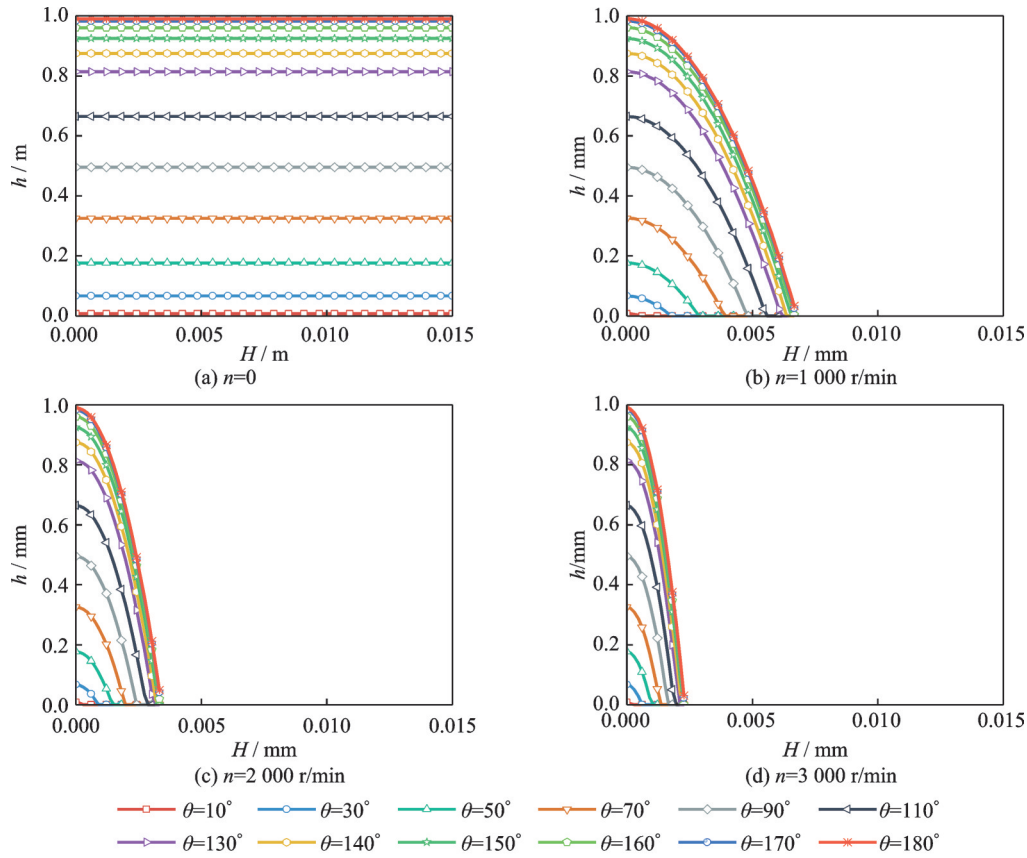


Fig.15 Relationship between critical liquid film thickness and bulge height under different rotational speeds and contact angles

uid film remains stagnant, while on rotating surfaces, obvious rivulets pattern. Secondly, comparing the effects of contact angle, overall, as the contact angle increases, the critical thickness and bulge height of water film/rivulet flow on rotating surfaces increase, indicating that a larger contact angle results in greater damping force on the water film/rivulet flow, and making it more difficult to flow on the surface. Therefore, bulges are more likely to form and rupture into discrete droplet flows. In addition, although a detailed analysis of the curves for different centrifugal radii is not performed, Eq.(8) reveals that the effect of centrifugal radius exhibits a trend similar to that of rotational speed. An increase in centrifugal radii increases the centrifugal force and aerodynamic drag on the water film/rivulet flow, reducing the critical thickness and bulge height, and making the water film/rivulet flow more prone to flow along the surface.

2.5 Theoretical model analysis of droplet flow based on FB method

During the runback flow process, the flow pat-

tern of the water film evolves, transitioning from a continuous film to rivulets, and further transforming into droplet flows that detach from the surface. The droplet flows can be approximated as droplets. Under aerodynamic drag, the detachment behavior of droplets on surfaces can be categorized into two modes: Sliding and lifting^[34]. In the sliding mode, the forces acting in the flow direction are analogous to those governing the water film/rivulet flows discussed in Section 2.4, so it will not be further elaborated here. The focus is primarily on the normal forces to analyze the impact of wettability on droplet detachment behavior. The force analysis of droplet flow lifting mode is conducted by selecting a droplet with a diameter of R_d as the analysis object. The droplet is mainly subjected to aerodynamic lift F_L , centrifugal force F_o , surface tension $F_{\sigma,y}$, and gravity F_g , in the direction perpendicular to the wall, as shown in Fig.16.

The FB in the direction perpendicular to the surface is

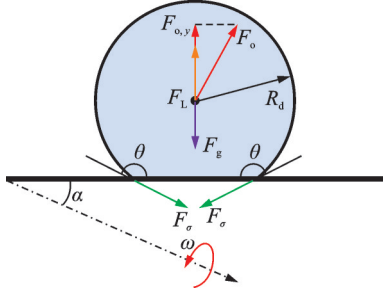


Fig.16 Physical model and force analysis of droplet flow on rotating surfaces

$$F_L + F_{o,y} = F_{\sigma,y} + F_g \quad (10)$$

$$\begin{cases} \frac{1}{2} \rho_g U_\infty^2 C_L \pi R_d + \frac{\pi}{3} \rho_l R_d^2 (2 - 3\cos\theta + \cos^3\theta) (\omega^2 r_o \cos\alpha - g) = 2\pi\sigma \sin^2\theta & 0^\circ < \theta < 90^\circ \\ \frac{1}{2} \rho_g U_\infty^2 C_L \pi R_d \sin^2\theta + \frac{\pi}{3} \rho_l R_d^2 (2 - 3\cos\theta + \cos^3\theta) (\omega^2 r_o \cos\alpha - g) = 2\pi\sigma \sin^2\theta & 90^\circ \leq \theta < 180^\circ \end{cases} \quad (15)$$

Eq.(15) can be used to determine whether droplet flow will lift off from the rotating surface. To simplify the equation for analysis, the operating condi-

$$\begin{cases} 154R_d \sin^2\theta + (847\omega^2 r_o - 10273) (2 - 3\cos\theta + \cos^3\theta) R_d^2 = 0.457 \sin^2\theta & 0^\circ < \theta < 90^\circ \\ 154R_d + (847\omega^2 r_o - 10273) (2 - 3\cos\theta + \cos^3\theta) R_d^2 = 0.457 \sin^2\theta & 90^\circ \leq \theta < 180^\circ \end{cases} \quad (16)$$

Fig.17 shows the relationship between the critical droplet radius and centrifugal radius for droplet

$$F_L = \begin{cases} \frac{1}{2} \rho_g U_\infty^2 C_L \pi R_d^2 \sin^2\theta & 0^\circ < \theta < 90^\circ \\ \frac{1}{2} \rho_g U_\infty^2 C_L \pi R_d^2 & 90^\circ \leq \theta < 180^\circ \end{cases} \quad (11)$$

$$F_{\sigma,y} = 2\pi R_d \sigma \sin^2\theta \quad (12)$$

$$F_{o,y} = \rho_l V_d \omega^2 r_o \cos\alpha =$$

$$\frac{\pi}{3} \rho_l R_d^3 (2 - 3\cos\theta + \cos^3\theta) \omega^2 r_o \cos\alpha \quad (13)$$

$$F_g = \rho_l V_d g = \frac{\pi}{3} \rho_l R_d^3 (2 - 3\cos\theta + \cos^3\theta) g \quad (14)$$

From the FB, we have

tions used in the experiments (wind speed $U_\infty = 20$ m/s, $\alpha = 36^\circ$, $C_L = 0.2^{[35]}$) and relevant physical parameters and constants are used, while Eq.(15) is

lifting under different rotational speeds and contact angles.

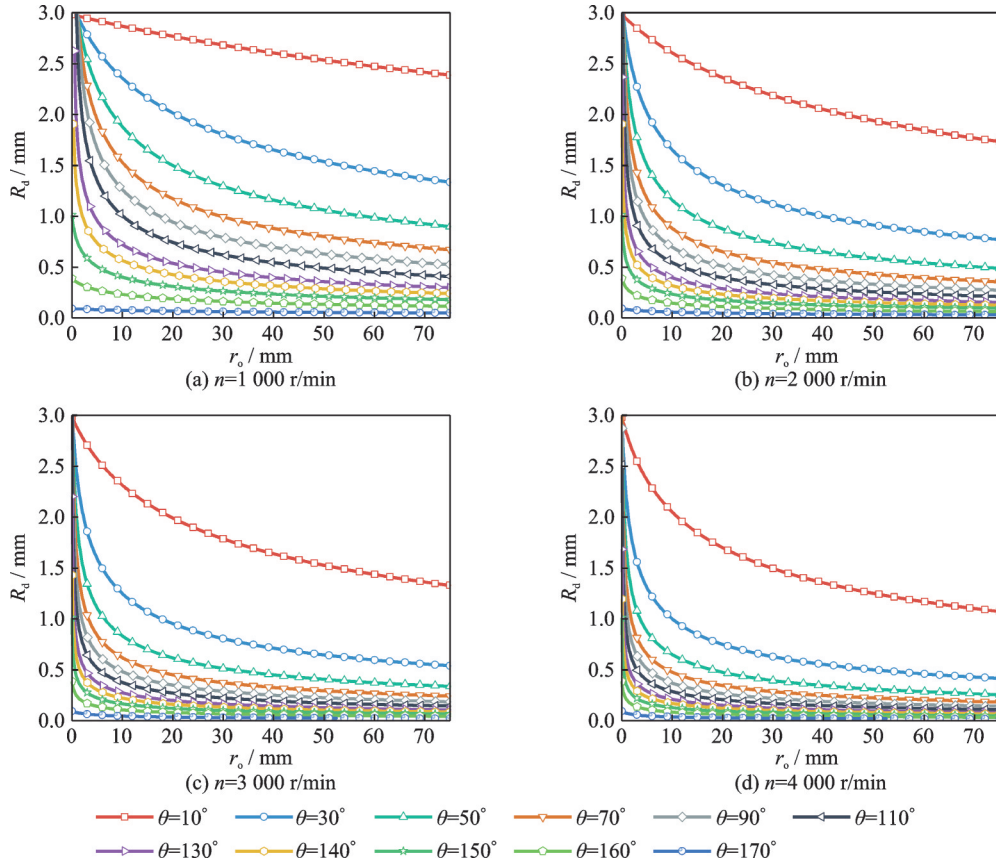


Fig.17 Relationship between critical droplet radius and centrifugal radius under different rotational speeds and contact angles

Overall, as the centrifugal radius increases, the critical droplet radius for lifting decreases. Therefore, on the rotating spinner surface studied in this paper, as the liquid water flows, the centrifugal radius continuously increases, and the droplet flow lifts off from the surface as the centrifugal force increases. Comparing Figs.17(a—d), as the rotational speed increases, the curves shift toward the origin, meaning that at the same centrifugal radius, the critical droplet radius decreases. For example, at a contact angle of 90° and a centrifugal radius of 30 mm, the critical droplet radius is 0.79 mm at a rotational speed of 1 000 r/min, but only 0.22 mm at a rotational speed of 4 000 r/min. The decrease in critical droplet radius means that droplet flows formed by water film rupture and breakup are more prone to lifting, and only smaller droplets can adhere to the surface, reducing the amount of liquid water coverage on the surface.

Secondly, comparing the results for different contact angles, as the contact angle increases, the critical droplet radius decreases at the same centrifugal radius, and droplets are more prone to lifting. Therefore, a larger contact angle results in a smaller liquid water coverage area on the surface. Additionally, on superhydrophobic surfaces with contact angles greater than 150° , the critical droplet radius for lifting is around $70\ \mu\text{m}$, and lifting can occur at a very small centrifugal radius. Therefore, on rotating superhydrophobic surfaces, large droplets are rarely observed adhering to the surface. The detachment of liquid water reduces the amount of water on the surface, fundamentally lowering the anti-icing heat load required for anti-icing and de-icing surfaces, thereby achieving low-energy anti-icing effects.

3 Conclusions

Surface wettability significantly affects the flow characteristics of runback water on rotating surfaces. This paper uses a VOF model in a rotating coordinate system to study the effects of wettability on runback water flow evolution characteristics on rotating surfaces. Furthermore, a theoretical model based on FB is developed, and the effects of surface wettability on water film evolution under different parameters on rotating surfaces is analyzed. The conclusions are summarized as follows:

(1) A 3D water flow simulation model on the rotating spinner is established using the VOF method and introducing a rotating reference frame. The simulation calculates the flow pattern of water films on four surfaces with different contact angles. The results show that runback water forms rivulets deflected opposite to the rotation direction in the middle of the spinner, and the rivulets flow runback and lift off from the surface as the centrifugal force increases.

(2) With an increase in contact angle, the more easily the water film breaks up into rivulets and droplet flows and the more likely it is to detach from the surface, thereby reducing the overall water film coverage. Similarly, as the rotational speed increases, the enhanced centrifugal force further facilitates film breakup and detachment, following a comparable trend.

(3) The analysis of the theoretical model reveals that as the rotational speed increases, the critical thickness and bulge height of the water film decrease, facilitating its flow along the rotating surface and promoting rivulet formation. Conversely, with an increase in contact angle, the damping force acting on the water film/rivulet increases, making surface flow more difficult while enhancing bulge formation and promoting its rupture into discrete droplet flows. During the runback process, as centrifugal force increases, droplet flows are more likely to lift off from the surface.

This study leaves several issues for further exploration: (1) The high computational cost of 3D water flow simulations using the VOF method necessitates the exploration of more efficient numerical approaches. (2) The ice accretion and shedding characteristics on rotating surfaces can be studied to explore the effectiveness of surface wettability in de-icing systems for rotating components.

References

- [1] LI Jing. Numerical simulation of ice accretion and study for icing scaling law on aero-engine entry components[D]. Xi'an: Northwestern Polytechnical University, 2015. (in Chinese)
- [2] CAO Y H, LI G Z, HESS R A. Helicopter flight characteristics in icing conditions[J]. The Aeronautical Journal, 2012, 116(1183): 963-979.
- [3] EDWARD B, JOSE P, EDWARD C S, et al. The Experimental investigation of a rotor hover icing model

- with shedding[J]. *OpenAlex*, 2010, 2: 1157-1173.
- [4] LIAN W L, XUAN Y M. Experimental investigation on a novel aero-engine nose cone anti-icing system[J]. *Applied Thermal Engineering*, 2017, 121: 1011-1021.
- [5] ZHAO L F, SHEN Y Z, LIU W L, et al. Solid-liquid-ice interfaces for anti-icing materials[J]. *Surfaces and Interfaces*, 2023, 42: 103510.
- [6] SUN Haoyang. Numerical and experimental investigation on anti-icing characteristics of superhydrophobic surface[D]. Beijing: Beihang University, 2023. (in Chinese)
- [7] MA Kuiyuan. Simulation and experimental investigation of aero-engine anti-icing based on superhydrophobic surfaces[D]. Beijing: Beihang University, 2024. (in Chinese)
- [8] MA K Y, LIN G P, JIN H C, et al. Experimental investigation of surface wettability induced runback water flow and heat transfer behavior[J]. *International Journal of Heat and Mass Transfer*, 2023, 209: 124164.
- [9] MA K Y, LIN G P, JIN H C, et al. Experimental investigation of runback water flow behavior on aero-engine rotating spinners with different wettabilities[J]. *Aerospace*, 2024, 11(7): 591.
- [10] YUAN Chaokai, LI Jinping, CHEN Hong, et al. Measuring method of overflow liquid film thickness in hypersonic flow[J]. *Scientia Sinica (Technologica)*, 2018, 48(6): 629-638. (in Chinese)
- [11] ZHANG K, HU H. An experimental study on the transient runback characteristics of wind-driven film/rivulet flows[J]. *Physics of Fluids*, 2021, 33(11): 112104.
- [12] MESSINGER B L. Equilibrium temperature of an unheated icing surface as a function of air speed[J]. *Journal of the Aeronautical Sciences*, 1953, 20(1): 29-42.
- [13] BOURGAULT Y, BOUTANIOS Z, HABASHI W G. Three-dimensional Eulerian approach to droplet impingement simulation using FENSAP-ICE, Part 1: Model, algorithm, and validation[J]. *Journal of Aircraft*, 2000, 37(1): 95-103.
- [14] MYERS T G, CHARPIN J P F, THOMPSON C P. Slowly accreting ice due to supercooled water impacting on a cold surface[J]. *Physics of Fluids*, 2002, 14(1): 240-256.
- [15] GORI G, PARMA G, ZOCCA M, et al. Local solution to the unsteady Stefan problem for in-flight ice accretion modeling[J]. *Journal of Aircraft*, 2018, 55(1): 251-262.
- [16] ZHENG M, DONG W, GUO Z Q, et al. Analysis of runback water flow on anti-icing surface using volume-of-fluid method[C]//*Proceeding of 2017 ASME Turbo Expo Turbine Technical Conference and Exposition*. Charlotte, North Carolina, USA: American Society of Mechanical Engineers, 2017.
- [17] THOMPSON B E, MARROCHELLO M R. Rivulet formation in surface-water flow on an airfoil in rain[J]. *AIAA Journal*, 1999, 37: 45-49.
- [18] EL-GENK M S, SABER H H. Minimum thickness of a flowing down liquid film on a vertical surface[J]. *International Journal of Heat and Mass Transfer*, 2001, 44(15): 2809-2825.
- [19] YANG Shiyu, CHANG Shinan, GAO Yanxin, et al. Investigation of rotary cone electric heating anti-icing transient process[J]. *Acta Aerodynamica Sinica*, 2016, 34(3): 289-294, 307. (in Chinese)
- [20] DONG W, ZHENG M, ZHU J, et al. Calculation and analysis of runback water flow on anti-icing airfoil surface[J]. *Journal of Aircraft*, 2016, 53(6): 1597-1605.
- [21] ZHU J, DONG W, ZHENG M, et al. Numerical investigation of heat and mass transfer on an anti-icing inlet cone[J]. *Journal of Propulsion and Power*, 2016, 32(3): 789-797.
- [22] JIAN Jinjin, JI Honghu, CAO Guangzhou, et al. Numerical study on water film flow and shedding in ice accretion of rotating spinner[J]. *Journal of Aerospace Power*, 2018, 33(11): 2725-2736. (in Chinese)
- [23] CHEN Ningli. Research on the prediction of movement and solidification of thin water film on a rotating surface and icing experiments[D]. Nanjing: Nanjing University of Aeronautics and Astronautics, 2018. (in Chinese)
- [24] CHEN X, ZHAO Q J. Numerical simulations for ice accretion on rotors using new three-dimensional icing model[J]. *Journal of Aircraft*, 2017, 54(4): 1428-1442.
- [25] WANG Z Z, ZHU C L. Study of the effect of centrifugal force on rotor blade icing process[J]. *International Journal of Aerospace Engineering*, 2017, 2017: 8695170.
- [26] WANG Z Z, ZHU C L. Numerical simulation for in-cloud icing of three-dimensional wind turbine blades[J]. *Simulation*, 2018, 94(1): 31-41.
- [27] HAMED A, DAS K, BASU D. Numerical simulations of ice droplet trajectories and collection efficiency on aero-engine rotating machinery[C]//*Proceedings of the 43rd AIAA Aerospace Sciences Meeting and Exhibit*. Reno, Nevada: AIAA, 2005.
- [28] WANG Z Z, ZHU C L. Numerical simulation of three-dimensional rotor icing in hovering flight[J]. *Proceedings of the Institution of Mechanical Engineers, Part G: Journal of Aerospace Engineering*, 2018, 232(3): 545-555.
- [29] HIRT C W, NICHOLS B D. Volume of fluid (VOF) method for the dynamics of free boundaries[J]. *Journal of Computational Physics*, 1981, 39(1): 201-225.

- [30] SAHOO S, ORPE A V, DOSHI P. Spreading dynamics of superposed liquid drops on a spinning disk[J]. *Physics of Fluids*, 2018, 30: 012110.
- [31] ZHOU Y, JIN Z Y, YANG Z G. Review on droplets impact process on moving and rotating surfaces[J]. *Journal of Zhejiang University (Engineering Science)*, 2023, 57(10): 2060-2076.
- [32] PENN D G, LOPEZ DE BERTODANO M, LYK- OUDIS P S, et al. Dry patch stability of shear driven liquid films[J]. *Journal of Fluids Engineering*, 2001, 123(4): 857-862.
- [33] KEITH T, DE WITT K. Development of an anti-icing runback model[C]//*Proceedings of the 28th Aerospace Sciences Meeting*. Reno, NV, USA: AIAA, 1990.
- [34] BASU S, NANDAKUMAR K, MASLIYAH J H. A model for detachment of a partially wetting drop from a solid surface by shear flow[J]. *Journal of Colloid and Interface Science*, 1997, 190(1): 253-257.
- [35] HÖLZER A, SOMMERFELD M. Lattice Boltzmann simulations to determine drag, lift and torque acting on non-spherical particles[J]. *Computers & Fluids*, 2009, 38(3): 572-589.

Acknowledgements This work was supported by the National Natural Science Foundation of China (No.12172029) and the open Research Project of Key Laboratory of Icing and Anti/De-icing of CARDC (No.IADL 20230101).

Authors

The first author Mr. ZHU Yuanxun received the B.S. degree in aerospace engineering from School of Aeronautic Science and Engineering, Beihang University, Beijing, China,

in 2023. Currently, he is pursuing the Ph.D. degree at Hangzhou International Innovation Institute, Beihang University. His research interests include aircraft icing and de-icing, wave-transmissive and electro-thermal coupling performance.

The corresponding authors Dr. MA Kuiyuan received the Ph.D. degree in man-machine and environmental engineering of Beihang University in 2024. Currently, he is working as a postdoctoral researcher at Hangzhou International Innovation Institute, Beihang University. His research focuses on the mechanisms of icing and anti/de-icing processes, as well as the development of advanced low-energy anti/de-icing technologies for aerospace applications. Prof. LIN Guiping is a Ph.D. Supervisor at School of Aeronautic Science and Engineering, Beihang University, and Director of the Key Laboratory of Man-Machine Ergonomics and Environmental Control. His main research focuses on aircraft environmental control and life support technology, aircraft anti/de-icing technology, and integrated aircraft energy management.

Author contributions Mr. ZHU Yuanxun complied the models, discussed and exchanged views, and wrote the manuscript. Dr. MA Kuiyuan designed the study, contributed to data and model components, interpreted the results, and contributed to the discussion and background of the study. Prof. LIN Guiping conducted content review and experiment management. Dr. JIN Haichuan assisted in obtaining project funding and arranged the progress of the study. Dr. BU Xueqin conducted the analysis of the simulation. All authors commented on the manuscript draft and approved the submission.

Competing interests The authors declare no competing interests.

(Production Editor: XU Chengting)

表面润湿性对发动机旋转帽罩上溢流水流动演化影响的三维数值模拟研究

朱元勋¹, 马奎元¹, 林贵平^{1,2}, 靳海川², 卜雪琴²

(1. 杭州市北京航空航天大学国际创新研究院(北京航空航天大学国际创新学院), 杭州 311115, 中国;

2. 北京航空航天大学航空科学与工程学院, 北京 100191, 中国)

摘要: 航空发动机进口部件在飞行中可能发生结冰从而影响运行安全。传统的热气防冰系统需要较大的引气量, 影响发动机性能, 因此基于超疏水表面的低能耗防除冰方法引起广泛关注。已有研究指出, 对于静止部件而言, 超疏水表面通过改变溢流水的流动行为, 显著减少了防冰能耗。然而, 对于发动机进口旋转部件, 由于离心力和科里奥利力的作用, 超疏水表面的有效性以及润湿性对溢流水流动演化的影响仍不清楚。本文采用VOF (Volume of fluid)方法建立了三维表面液态水流动仿真模型, 研究了动态旋转条件下转速、风速、表面润湿性对三维旋转帽罩上溢流水流动的影响。结果表明, 旋转效应和表面润湿性相互促进, 转速和接触角的增大都能够沿表面方向上提高液态水的流动速度, 并加速液膜破裂形成湍流、珠状流并脱离表面的过程。通过受力平衡分析了流动演化过程以及旋转效应和润湿性对于旋转表面水膜流动演化行为的耦合作用。分析表明, 随着转速和接触角增大, 水膜更容易破裂形成湍流、珠状流, 液滴发生飞离的临界半径减小, 更易脱离表面。

关键词: 防冰; 溢流水特性; VOF; 表面润湿性; 旋转表面